X-690-75-32

PREPRINT

NASA TM X- 70832

# THE MAGNETIC FIELD OF MERCURY: PART ONE



N. F. NESS

K. W. BEHANNON

R. P. LEPPING

Y. C. WHANG



NOVEMBER 1974

GSFC

GODDARD SPACE FLIGHT CENTER

GREENBELT, MARYLAND

For information concerning availability
of this document contact:

Technical Information Division, Code 250
Goddard Space Flight Center
Greenbelt, Maryland 20771

(Telephone 301-982-4488)

# THE MAGNETIC FIELD OF MERCURY: PART I

N. F. Ness
K. W. Behannon
R. P. Lepping
Laboratory for Extraterrestrial Physics
NASA/Goddard Space Flight Center
Greenbelt, Md. 20771

Y. C. Whang
Catholic University
Washington, D. C.

(In Press, J. Geophys. Res., 1975)

November 1974

# THE MAGNETIC FIELD OF MERCURY: PART I

by

N. F. Ness
K. W. Behannon
R. P. Lepping
Y. C. Whang

Abstract

An updated analysis and interpretation is presented of the magnetic field observations obtained during the Mariner 10 encounter with the planet Mercury on 29 March 1974. The combination of data relating to position of the detached bow shock wave and magnetopause, and the geometry and magnitude of the magnetic field within the magnetosphere-like region surrounding Mercury, lead to the conclusion that an internal planetary field exists with dipole moment approximately $5.1 \times 10^{22}$ Gauss-cm$^3$. The limited data set precludes quantitative determination of an intrinsic field more complex than a centered dipole. The dipole axis has a polarity sense similar to Earth's and is tilted $7^{\circ}$ from the normal to Mercury's orbital plane. The magnetic field observations reveal a significant distortion of the modest Hermean field (350$\gamma$ at the equator) by the solar wind flow and the formation of a magnetic tail and neutral sheet which begins close to the planet on the night side. Presently, an active dynamo mechanism in the planetary interior appears favored in the interpretation of the field origin, although fossil remanent magnetization cannot be excluded. The composite data set is not consistent with a complex induction process driven by the solar wind flow.

INTRODUCTION

The first in-situ measurements of the solar wind interaction with the planet Mercury and its magnetic field were performed by the Mariner 10 spacecraft on 29 March 1974. A preliminary report (Ness et al, 1974b) presented the initial results of the analysis of data obtained from the dual magnetometer experiment. The unexpected observation of a very well developed, strong detached bow shock wave was interpreted as being due to the existence of a modest magnetosphere-like region associated with an intrinsic magnetic field of the planet. Simultaneous measurements of the low energy electron flux ($13.4 < E_e < 687$ ev) by Ogilvie et al. (1974) provided strong correlative evidence for this interpretation. In addition, intense bursts of higher energy electrons ($E_e > 170$ Kev) and protons ($E_p > 500$ Kev) were reported by the charged particle telescope experiment (Simpson et al., 1974) as occurring in a region of space corresponding to the magnetosphere and magnetosheath following Mariner 10's closest approach to Mercury.

The previous report by Ness et al. (1974b) also discussed the possibility of a complex induction mode, due to solar wind transport of the interplanetary field past the planet, leading to the set of observations obtained. A review of the arguments presented then against the induction mode hypothesis does not indicate any need at the present time for further consideration. The combination of factors relating to the geometry and positions of the bow shock and magnetopause, which implies a scale size of solar wind interaction larger than the planet, and both the geometry and magnitude of the magnetic field within the magnetosphere-like region are found to be inconsistent with present models of such planetary interactions. The lack of evidence for

any appreciable atmosphere or ionosphere (Broadfoot et al., 1974; Howard et al., 1974) suggests that the interaction is unlike that at Venus, wherein a substantial atmosphere-ionosphere is responsible for the deflection of the solar wind flow and the development of the detached bow shock wave (Bridge et al., 1974; Ness et al., 1974a).

A unique feature of the Mariner 10 heliocentric orbit is that following the gravity assist at Venus, the orbital period is exactly twice Mercury's period so that on 21 September 1974 a second encounter with the planet occurred. The targeting strategy for that encounter was biased to provide optimum imaging coverage of the south polar regions, and so the spacecraft did not approach sufficiently close to the planet (minimum distance $\approx 5 \times 10^4$ km) to directly observe the magnetic field of the planet and/or any effects associated with the solar wind interaction. A third encounter will occur on 16 March 1975, and appropriate targeting plus successful spacecraft performance should permit additional observations of the magnetic field environment and solar wind interaction with the planet Mercury.

It is the purpose of this report to present a brief review of the magnetic field observations and the updated final result of the quantitative analysis of the first encounter data yielding an estimate of the intrinsic magnetic field of the planet Mercury.

MAGNETIC FIELD OBSERVATIONS

Detailed data obtained near Mercury I encounter are presented in Figure 1. Individual data points used in this figure represent a reconstituted vector magnetic field obtained from 1.2 second component averages utilizing the 25 Hz vector magnetic field sampling rate of the instrument. Details regarding the accuracy of magnetic field measurements obtained with the dual magnetometer system on this, its first flight, have already been presented (Ness et al., 1974a). The data in Figure 1 illustrate very clearly the important features of the magnetic field measurements. A multiple crossing of the bow shock occurs between 2027 UT and 2028 UT 29 March 1974. It is well identified both by the abrupt increase in average field magnitude and the increase in the fluctuating magnetic field, as measured by the RMS parameter.

The magnetopause is well distinguished by the abrupt directional change in the magnetic field, noted primarily in the $\phi$ curve, but also is reflected in the abrupt termination of high frequency fluctuations measured by the RMS parameter. The average field magnitude is observed to increase across the magnetopause. Between this boundary crossing and closest approach the magnetic field is seen to be rather steady in direction, especially with respect to higher frequency fluctuations. It is noted that between 2040 UT and 2046 UT the magnetic field fluctuations are substantially less than in the magnetosheath and even markedly smaller than in the interplanetary medium. Small amplitude, $<5\gamma$, and longer period fluctuations, periods greater than a few seconds, are observed in this portion of the magnetosphere.

Following closest approach, abrupt and large variations of the magnetic

field are observed. It is important to note in this data presentation that although the field magnitude varies by up to 50% from its average value throughout the data set up to the outbound magnetopause crossing, the general direction of the magnetic field does not change. In other words, an average direction of the magnetic field exists during this period of time which is not destroyed by the large amplitude fluctuations of the magnetic field. The rapid time variations of the magnetic field following closest approach and the associated electron flux measurements have been interpreted in terms of a substorm which disturbed the Hermean magnetosphere in association with a southward turning of the interplanetary magnetic field during the encounter (Siscoe, Ness and Yeates, 1975).

The identification of the outbound magnetopause near 2054 UT is based on a large directional change in the magnetic field from a large positive $\theta$ to large negative $\theta$. Subsequently, the spacecraft remains in the rather disturbed magnetosheath until the bow shock crossings are observed. The identification of the outbound bow shock crossing is much less distinctive than inbound due both to the disturbed nature of the Hermean magnetosphere at this time as well as the orientation of the interplanetary magnetic field. As previously discussed by Ness et al. (1974b), the contrast is due to the different relative orientations of the interplanetary magnetic field. It was nearly orthogonal to the bow shock surface normal when Mariner 10 was inbound and conversely was rather more parallel outbound.

The data obtained within the magnetopause crossings are presented in a different format in Figure 2. Here 42 second average vector components are plotted in 2 different planes, as viewed from the sun along the -X axis and as projected on a plane parallel to the ecliptic. In the lower portion of the

figure, the traces of a magnetopause and bow shock boundary, scaled for the case of a dipole magnetic moment of Mercury equal to $7 \times 10^{-4}$ of Earth's moment, are included. A few of the vectors representing observations outside the magnetopause, when the spacecraft was within the magnetosheath, are also shown to illustrate the sharp and distinctive change in the field direction which occurs at these boundaries.

The quiet interval of the magnetosphere observations is identified, and there the magnetic field has a directional sense analogous to that of the Earth's magnetosphere on the near dark side. In that region of space, the magnetic tail is beginning to develop. While the large scale disturbances of the magnetic field occurring after closest approach are readily evidenced in the lower portion of the figure, the preservation of the magnetic field direction previously referenced is illustrated in the upper portion of the figure with the field being roughly parallel to the +Z-axis and positive throughout.

It is instructive to compare these data presentations with Figure 3, which illustrates the general characteristics of the external magnetic fields which result from the solar wind interaction with the geomagnetic field. As the solar wind is deflected around the Earth, whose dipole is almost perpendicular to the flow of solar wind, the nominal stagnation point of flow occurs at 10 earth radii, and the geomagnetic field is confined to a region of space originally called the Chapman-Ferraro cavity and now known as the magnetosphere. Electrical currents which flow on the surface of the magnetosphere, i.e. in the magnetopause, are responsible for the abrupt change in direction which is characteristically observed in the magnetic field as a spacecraft crosses this surface.

On a larger scale, these fields extend throughout the magnetosphere with approximately the geometry shown. In addition, the development of the geomagnetic tail and embedded neutral sheet is due to a second system of electrical currents whose magnetic field can be described as having an origin associated with the tail of the magnetosphere.

Note that these external fields have a rather specific directional characteristic. Below the plane of the equator and neutral sheet, which are assumed coincident in this figure, the component parallel to the Sun-earth line is always directed in an anti-solar sense, while above that plane it points sunward. However, the field component parallel to the dipole axis depends upon the observer's position relative to the boundary of the Chapman-Ferraro cavity and to the magnetic tail neutral sheet, but is never observed to reverse polarity.

From studies of the earth's magnetosphere, it is known that in the immediate vicinity of the neutral sheet a region of significantly weakened magnetic field strength is always measured coincident with the change of the sign of the component parallel to the earth-Sun line.

The magnetic field observations by Mariner 10 show a rather good correspondence to the earth's magnetosphere if an appropriate scaling of sizes is taken into account. With the stagnation point of solar wind flow inferred to be at 1.6 $R_{\mu}$, then the scaling yields the results shown in Figure 3. There it is seen that the planet Mercury occupies a very large fraction of the volume of the magnetosphere. Thus, even when measurements are performed relatively close to the surface of the planet, the total field includes a substantial part due to the external sources. This is quite unlike the situation for near-earth orbiting spacecraft.

It is this fact, coupled with a very limited data set available in a restricted volume of the magnetosphere sampled by Mariner 10, which limits the ability to properly analyze the data in terms of an intrinsic internal planetary magnetic field. While quantitative models describing the magnetic field in the terrestrial magnetosphere exist, their results are generally sensitive to the choice of parameter values employed when in close proximity to either the magnetopause or neutral sheet. Away from these regions, that is, in the well developed geomagnetic tail or within 8 earth radii, the models are moderately successful in describing the asymmetry of the radiation belts, the polar cap regions and associated phenomena.

It is not necessary that we attempt to determine a magnetic field representation valid throughout the entire Hermean magnetosphere in order to estimate the intrinsic planetary field. What is needed is a proper representation along the trajectory and then to ascertain whether or not the internal field thus obtained provides a consistent description of the Hermean magnetosphere and its interaction with the solar wind. The next section presents such an analysis.

LEAST SQUARES DATA FIT

In the preliminary report on these results (Ness et al., 1974b), the very simplified representation of the magnetic field as due entirely to an offset, tilted magnetic dipole was made and no external sources of field were considered. Using only quiet interval data, immediately surrounding closest approach, a reasonable data fit was obtained with an RMS of ~10$\gamma$ based upon an offset dipole of magnitude $3.3 \times 10^{22}$ Gauss-cm$^3$, oriented at latitude $-70^\circ$ and longitude $209^\circ$. This moment was 40% smaller than that inferred from the position of the bow shock and magnetopause, $5.6 \times 10^{22}$ Gauss-cm$^3$. It was compensated by the moderately large offset: 0.47 $R_\varphi$ at a latitude $\theta = +17^\circ$ and longitude $\phi = 62^\circ$.

Unfortunately, the magnetic field data set which is available for analysis is incomplete in a mathematical sense. The unique determination of the characteristics of that portion of the observed magnetic field which can be ascribed to the interior of the planet demands a set of vector observations over a simple surface enclosing the planet, for example on a sphere. In the absence of such a data set, it is necessary to make additional assumptions regarding the nature of the magnetic field characteristics in order to estimate the interior field.

Since there is no evidence for the existence of a permanently trapped radiation belt (Simpson et al., 1974) nor an ionosphere (Howard et al, 1974), we assume that the region of space between the surface of the planet and the magnetopause boundary is devoid of any significant electrical currents except for the neutral sheet in the tail. This permits the use of a scalar potential to define the magnetic field in this source free region. Using the traditional spherical harmonic

representations employed in geomagnetic field analyses, the magnetic field potential, V, is represented by the following expression:

$$V = a\sum\sum\left\{\left(\frac{a}{r}\right)^{n+1}\left[g_n^m \cos\ m\phi + h_n^m \sin m\phi\right] + \left(\frac{r}{a}\right)^{n}\left[G_n^m \cos\ m\phi + H_n^m \sin m\phi\right]\right\} P_n^m (\cos\theta),$$

and $\vec{B} = -\nabla V$ .

Here $g_n^m$, $h_n^m$ represent internal sources, $H_n^m$, $G_n^m$ represent external sources and a = radius of the planet. Note that here $\theta$ is measured from the pole of the coordinate system (the +Z axis) and not the equator, as is the case in the presentation of field data in this paper.

Since the data are available only in a very limited region of space along the spacecraft trajectory, and indeed since the quiet magnetosphere exists for only one half of the spacecraft's residence time within the magnetosphere, it is not reasonable to expect to be able to determine harmonic coefficients of high degree in any such analysis.

The approach used has been to assume internal sources described by terms of degree n = 1, which means a centered magnetic dipole. Even if the planet possesses an offset dipole, the n = 1 coefficients would be unchanged but terms of degree n = 2 and greater would appear. The external sources of the field are assumed to be adequately represented by harmonics up to and including degree n = 2. A uniform external field is represented by the terms corresponding to n = 1. A least squares fit has been made to the data using different sets of contiguous data points within the quiet interval; note that the data points used in this analysis were 42 second averages. Identifying the data points within the

magnetosphere in ascending numerical order from 1 to 25, it has been found that use of data points 4-13 gives results which are quite representative of the entire quiet data set, represented by data points 1 - 13.

The least squares fit to the three orthogonal components is accomplished by a classical minimization process for the Pythagorean mean of the field components. That is: a minimum of $\sum(\vec{B}_{obs}-\vec{B}_{th})\cdot(\vec{B}_{obs}-\vec{B}_{th})$ is sought. The results obtained for the internal dipole coefficients are as follows:

$$g_1^0 = -344$$

$$g_1^1 = +16$$

$$h_1^1 = -59$$

The fit to the data points (RMS = 1$\gamma$) is illustrated graphically in Figure 4. Here it is seen that the spherical harmonic representation fits the data very well during the quiet period of magnetosphere traversal. Another combination of harmonic coefficients has been investigated, which assumed a higher degree of complexity of the internal planetary field (i.e. $n_{int}\leq 2$) and a reduced complexity of the external field (i.e. $n_{ext}=1$). The results so obtained were rather sensitive to the specific set of data points used which suggested a less physically plausible representation.

From the above harmonic coefficient set, it is found that the intrinsic field of the planet is represented as due to a centered dipole of moment $5.1 \times 10^{22}$ Gauss-cm$^3$ oriented at a solar ecliptic latitude of $-80^\circ$ and longitude $+285^\circ$. This moment compares very well with that deduced from the positions of the magnetopause and bow shock boundaries and the inferred magnetic moment responsible for solar wind deflection. The orientation is approximately the same but the magnitude is rather larger than that of the offset dipole obtained in the preliminary analysis. The discrepancy in dipole magnitude and location is easily understood in terms of the significant contributions of external sources, which were given no representation in the preliminary undistorted dipole field model.

It is not to be expected that the above harmonic representation of the magnetic field is valid throughout the entire Hermean magnetosphere. Rather it should be clear that the representation is constrained to the vicinity of the spacecraft trajectory. On the other hand, the internal magnetic field of the planet can be extrapolated to permit computation of the magnetic field perturbations associated with the solar wind interaction and the magnetosphere temporal disturbance.

These magnetic field perturbation vectors are presented in Figure 5, using the same format as in Figure 2. The characteristics of the perturbation field are clearly illustrated for both the quiet period in the magnetosphere as well as the disturbed period. Note that the perturbation magnetic field, when viewed from the sun, is always pointed "southward" throughout the entire trajectory passage through the magneto-

sphere. In the lower portion of the figure, the sense of the perturbation field is initially anti-solar just following the inbound magnetopause crossing but then swings around until, simultaneous with the disturbance of the magnetosphere, it becomes solar directed.

In comparing this perturbation field with models of the disturbed geomagnetic field due to solar wind interaction (see Figure 3), one is compelled to draw an analogy with the existence of a neutral sheet on the dark side of Mercury due to the formation of a magnetic tail as the solar wind interacts with the planet. The spacecraft trajectory was such that Mariner 10 entered the magnetosphere below the neutral sheet and was in close proximity to it at closest approach. Thereafter, the spatial position of the spacecraft and temporal changes of the magnetosphere combined to place Mariner 10 above the extrapolated position of the neutral sheet as it exits the magnetosphere. The abrupt decrease and recovery from 2047 to 2048 UT seen in Figure 1 may be due to an intensification of the neutral sheet current as the tail field increases and/or a motion of the edge of the neutral sheet closer to the planet.

It should be remarked that the above analysis and interpretation lead to a situation wherein the perturbation magnetic field is a large fraction of the inferred intrinsic field of the planet. For example, at the last data point in the quiet interval, the Z component of the perturbation field is -109$\gamma$, 80% of the dipole field, +140$\gamma$. Its polarity is opposite to the internal field, and this is consistent with the general topology of the magnetic field of the magnetosphere of Mercury being similar to the Earth's.

IMPLICATIONS

The existence of both a modest magnetic field of Mercury sufficient to deflect the solar wind and an imbedded neutral sheet lead to the conclusion that there should exist a magnetic tail of Mercury. The possible characteristics of such a magnetic tail are illustrated in Figure 6. Assuming that the magnetic flux in the polar regions of the planet connect with the tail and that negligible merging takes place across the neutral sheet, one can infer the size of the polar cap region.

Measurements of the magnetic field just after the inbound magnetopause crossing suggest that for Mercury the tail field is 30 to 40$\gamma$ with a radius of approximately 2.05 to 2.6 $R_{\mu}$. With the assumed magnetic dipole moment of $5.1 \times 10^{22}$ Gauss-$cm^3$ for the planet, this leads to a polar cap co-latitude of 18 to 26 degrees, approximately twice that of the earth's.

The optical properties of the Hermean surface are similar in many respec to those of the moon (Hameen-Anttila et al., 1970; McCord and Adams, 1972). The lunar surface optical properties are influenced most by size, composition and structure but also by ion bombardment by the solar wind. It is believed that the flux of solar wind ions impacting the lunar surface leads to a darkening of surfacial material (Hapke, 1971). With this point in mind, then it becomes necessary to investigate whether or not the magnetic field inferred for Mercury is such that it would always deflect the solar wind flow from the planetary surface.

The preliminary interpretation of a tilted dipole with appreciable offset led naturally to a situation in which the solar wind periodically

could impact the surface during each planetary orbit. The present interpretation, using a centered dipole, yields a value of magnetic dipole which is sufficient to deflect the solar wind momentum flux at most times during the planetary orbit except those when the solar wind flux is higher than average when the planet is near perihelion.

Figure 7 illustrates the relationship between solar wind momentum flux, equatorial field strength, $B_o$, and radius of the subsolar magnetopause, $R_{mp}$, in units of planetary radius $R_p$. It has already been deduced (Ness et al., 1974b) that at the Mercury I encounter, the solar wind momentum flux of $1.1 \times 10^{-7}$ dynes/cm ($\pm 10\%$) and the inferred standoff distance of 1.6 $R_p$ lead to an intrinsic equatorial field strength of $380 \pm 32\gamma$. If the solar wind momentum flux increases by a factor of 5, then the magnetopause is pushed down to 1.2 $R_{\mathrm{Mercury}}$, which is less than 500 km above the surface. On this scale, the fluid approximation to solar wind flow begins to break down because of the finite size of the cyclotron radius, 50-100 km, and the finite thickness of the magnetopause. A further increase in solar wind flux leads to a situation wherein the solar wind ions approach within 1 gyro radius of the planetary surface, so that the deflection of the flow would be incomplete as the solar wind begins to directly impact and be absorbed by the planetary surface. It should be noted that, in analogy with the earth, solar wind and more energetic particles have direct access to the planet through the polar cap and neutral sheet.

SUMMARY AND CONCLUSIONS

An improved quantitative analysis of the magnetic field data obtained by Mariner 10 during the Mercury I encounter on 29 March 1974 is presented. The limited data available during the time interval when the magnetosphere-like region was in a steady state condition restricts the ability to uniquely evaluate the nature of the planetary field. Assuming a centered magnetic dipole for the intrinsic field of the planet and attributing the distortion of the dipole field to fields associated with external sources whose complexity is well represented by harmonics up to degree 2, a least squares analysis yields an excellent fit (RMS = 0.95$\gamma$) and a very self consistent interpretation to the composite data set.

The intrinsic magnetic field dipole moment is found to be $5.1 \times 10^{22}$ Gauss-cm$^3$, oriented in a polarity sense similar to Earth's dipole and at SE solar ecliptic $\theta = -80^\circ$ and $\phi = 285^\circ$. Subtracting this intrinsic field from the observed field yields a perturbation field, due to magnetopause and magnetotail currents, whose characteristics are similar to the spatial and also temporal distortion of the magnetosphere as in the Earth's case. The dipole axis is tilted only $7.2^\circ$ from the normal to Mercury's orbital plane and thus within $4^\circ$-$10^\circ$ of the rotation axis.

A fundamental question unresolved is that of the origin of this global intrinsic planetary field. At the present time, we do not believe the data support theories invoking a complex induction source mechanism due to the flow of the solar wind. Two possible alternatives are: a present day active dynamo or fossil magnetization due to an ancient dynamo or an enhanced interplanetary magnetic field during cooling. Both depend upon the thermal state of the planetary interior and it is not possible to distinguish between the two mechanisms. Partially this is due to our lack of a precise model for a planetary dynamo (Stevenson, 1974)

and also to the lack of information concerning the structure of the planetary interior. Due to the high average density of the planet, 5.44 gms/cc, it is fairly certain that a large amount of iron exists, on the order of 60%, which is probably concentrated in a large core (Kozlovskaja, 1969; Plagemann, 1965; Reynolds and Summers, 1969; Siegfried and Solomon, 1974; Toksoz and Johnston, 1975). If such a core were at low temperatures, below the Curie point, then a remanent magnetic field is quite plausible, although then the problem is to determine the origin of the magnetizing field.

The possibility of a sufficiently cold core seems very remote in the light of studies on the thermal evolution of the terrestrial planets. Toksoz and Johnston (1975) have shown that early in Mercury's history a substantial iron nickel core formed with a radius of approximately 1600km. Such a large core can probably support a planetary dynamo, if the appropriate combination of fluid motions and electrical properties exist. While the slow rotation of the planet may appear to be an impediment to the successful application of dynamo theory, the important physical parameters for a dynamo include dimensionless numbers for flattening, the differential rotation of the planetary interior, the magnetic Reynolds number, and other such quantities. We do not believe sufficient data exists at present which can uniquely exclude an active dynamo from further consideration for the origin of the magnetic field. It does appear doubtful that the decay of an ancient dynamo could have a time constant long enough to sustain the field, based on any reasonable estimate of core electrical conductivity and magnetic permeability.

With a warm or hot interior, the question arises as to whether or not fossil magnetization of a thin solid mantle would be possible. Again,

the absence of definitive information on the thermal characteristics of near surface material precludes an answer to this question. However, it is instructive to consider the magnitude of remanent magnetization required, in spite of the probable high near surface temperatures. Assuming a uniformly magnetized thin spherical shell, the magnetization required is not much larger than the remanent magnetizations found in the returned lunar samples (Fuller, 1974). With a lithospheric shell below the Curie point whose thickness is 20% of the radius, 488 km, the necessary magnetization is $3.1 \times 10^{-4}$ emu/gram. For 10%, 244 km, the value rises to $5.9 \times 10^{-4}$ emu/gram. This is well within the range of materials which may be expected to be present on the planet Mercury, since lunar surface materials yield magnetizations generally within an order of magnitude of $10^{-5}$ emu/gram, but at much lower temperatures.

In the light of the limited data set available, it is not uniquely possible to choose between these two sources of magnetic field: active dynamo or fossil magnetism. As yet there is no agreement on whether the thermal history of Mercury includes the evolution of a fluid core (Majeva, 1969; Plagemann, 1965; Siegfried and Solomon, 1974) and whether there exists a lithospheric shell whose temperatures are below the Curie point. Perhaps additional data obtained during Mercury III encounter on 16 March 1975 will illuminate more clearly the quantitative characteristics of the planetary field, and hence its origin.

ACKNOWLEDGEMENTS

We appreciate the efforts of Mr. Richard Thompson of GSFC in the analysis of the data.

REFERENCES

Bridge, H. S., A. J. Lazarus, J. D. Scudder, K. W. Ogilvie, R. E. Hartle, J. R. Asbridge, S. J. Bame, W. C. Feldman, and G. L. Siscoe, Science, 183, 1293, 1974.

Broadfoot, A. L., S. Kumar, M. J. S. Belton and M. B. McElroy, Mercury's Atmosphere from Mariner 10: Preliminary Results, Science 185, 166, 1974.

Bullard, E., Geomagnetic Dynamics in the Application of Modern Physics to the Earth and Planetary Interiors, edited by S. K. Runcorn, pg.232, Wiley and Sons, New York, 1969.

Choe, J. T, D. B. Beard and E. E. Sullivan, Precise Calculation of the Magnetosphere Surface for a Tilted Dipole, Planet. Space Sci., 21, 485, 1973.

Fuller, M., Lunar Magnetism, Rev. Geophys. Space Phys., 12, 23, 1974.

Hameen-Anttila, K. A., T. Pikkarainen and H. Gaultchel Photometric Studies of the Planet Mercury, The Moon, 1, 440, 1970.

Hapke, B., Optical Properties of the Lunar Surface in Physics and Astronomy of the Moon, edited by Z. Kopal, 2nd Edition, pg.155, Academic Press, N.Y., 1971.

Howard, H. T., et al, Mercury: Results on Mass, Radius, Ionosphere and Atmosphere from Mariner 10 Dual Frequency Radio Signals, Science, 185, 179-180, 1974.

Kozlovskaya, S. V., On the Internal Constitution and Chemical Composition of Mercury, Astrophys. Letters, 4, 1, 1969.

Majeva, S. V., The Thermal History of the Terrestrial Planets, Astrophys. Letters, 4, 11, 1969.

McCord, T. B. and J. B. Adams, Mercury: Interpretation of Optical Observations, Icarus, 17, 585-588, 1972.

Ness, N. F., K. W. Behannon, R. P. Lepping, Y. C. Whang and K. H. Schatten, Magnetic Field Observations Near Venus: Preliminary Results from Mariner 10, Science, 183, 1301, 1974a.

Ness, N. F., K. W. Behannon, R. P. Lepping, Y. C. Whang, and K. H. Schatten, Magnetic Field Observations near Mercury: Preliminary Results, Science, 185, 151, 1974b.

Ogilvie, K. W., J. D. Scudder, R. E. Hartle, G. L. Siscoe, H. S. Bridge, A. J. Lazarus, J. R. Asbridge, S. J. Bame and C. M. Yeates, Observations at Mercury Encounter by the Plasma Science Experiment on Mariner 10, Science, 185, 145, 1974.

Plagemann, S., A Model of the Internal Constitution and Temperature of the Planet Mercury. J. Geophys. Res., 70, 985, 1965.

Reynolds, R. and A. Summers, Calculations on the Composition of the Terrestrial Planets, J. Geophys. Res., 74, 2494-2511, 1969.

Simpson, J. A., J. H. Eraker, J. E. Lamport and P. H. Walpole, Electrons and Protons Accelerated in Mercury's Magnetic Field, Science, 185, 160. 1974.

Siscoe, G., N. F. Ness and C. M. Yeates, Substorms on Mercury? Geophys. Res. Letters, to appear, 1975.

Siegfried, R. W. and S. C. Solomon, Mercury: Internal Structure and Thermal Evolution, Icarus, 23, 192, 1974.

Stevenson, David, Planetary Magnetism, Icarus, 22, 403, 1974.

Toksoz, M. N., and D. H. Johnston, The Evolution of the Moon and the Terrestrial Planets, Proceedings of the Soviet-American Conference on the Moon and Planets, 1975, in press.

FIGURES

Figure 1 Magnetic field data averages for 1.2 second periods during encounter in spacecraft-centered solar ecliptic coordinates. The latitude of the reconstituted vector is represented by $\theta$ and longitude by $\phi$, the field intensity by $\bar{F}$ while RMS represents the Pythagorean mean of the X, Y, Z component root mean square deviations. The X axis is directed to the Sun, the Z axis to north ecliptic pole and the Y azis completes the right handed coordinate system.

Figure 2 Observed 42 second average magnetic field vectors superimposed on trajectory of Mariner 10 in X-Z (top) and X-Y (bottom) planes during transit of Hermean magnetosphere. The actual magnetopause crossings are identified, along with the detached bow shock observations. The boundaries represent a best graphical fit obtained by scaling the case of the solar wind interaction with the Earth for $M = 7 \times 10^{-4}$ of the Earth's magnetic moment. $R_{\varphi} = 2439$ Km.

Figure 3 Sketch in noon-midnight meridian plane of secondary magnetic fields generated by the deflection of solar wind flow around geomagnetic field and extension of polar cap magnetic flux to form magnetic tail. For comparison, the size of Mercury within its magnetosphere is shown.

Figure 4 Three components of magnetic field data, during Hermean magnetosphere transit, represented by 42 second averages and a least squares fit of a spherical harmonic representation yielding a coefficient set describing the "quiet" interval with a RMS = $0.95\gamma$.

Figure 5 Perturbation magnetic field (observed field minus internal dipole field) due to external sources, superimposed on trajectory of Mariner 10 in X-Z (top) and X-Y (bottom) planes during transit of Hermean magnetosphere. See Figure 2 for comparison with observed field.

Figure 6 Relationship of magnetic tail field intensity, $B_T$, to radius of tail, $R_T$, as function of polar cap colatitude assuming centered internal dipole with moment = $5.1 \times 10^{22}$ Gauss-$cm^3$.

Figure 7 Relationship between equatorial field strength, $B_o$ (for a planetary field modeled by a magnetic dipole perpendicular to solar wind velocity) and distance to stagnation point, $R_{MP}$, normalized by planetary radius, $R_p$, for various values of deflected solar wind momentum flux $mnV^2$. Theoretical relationship given by Choe et al, (1973).

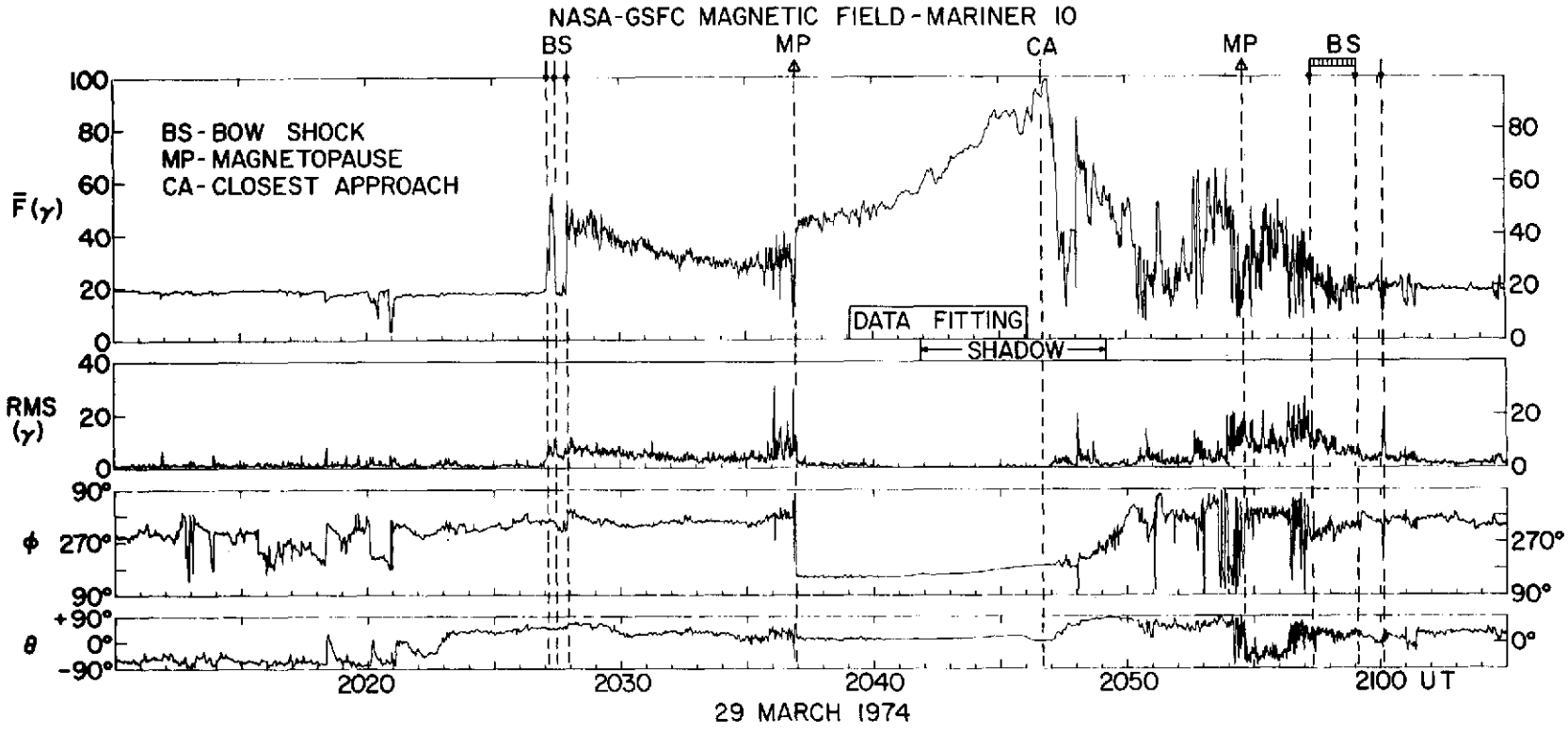
NASA-GSFC MAGNETIC FIELD - MARINER 10
BS
MP
CA
MP
BS
BS - BOW SHOCK
MP - MAGNETOPAUSE
CA - CLOSEST APPROACH
$\bar{F}(\gamma)$
DATA FITTING
SHADOW
RMS (γ)
φ
θ
2020
2030
2040
2050
2100 UT
29 MARCH 1974

FIGURE 1

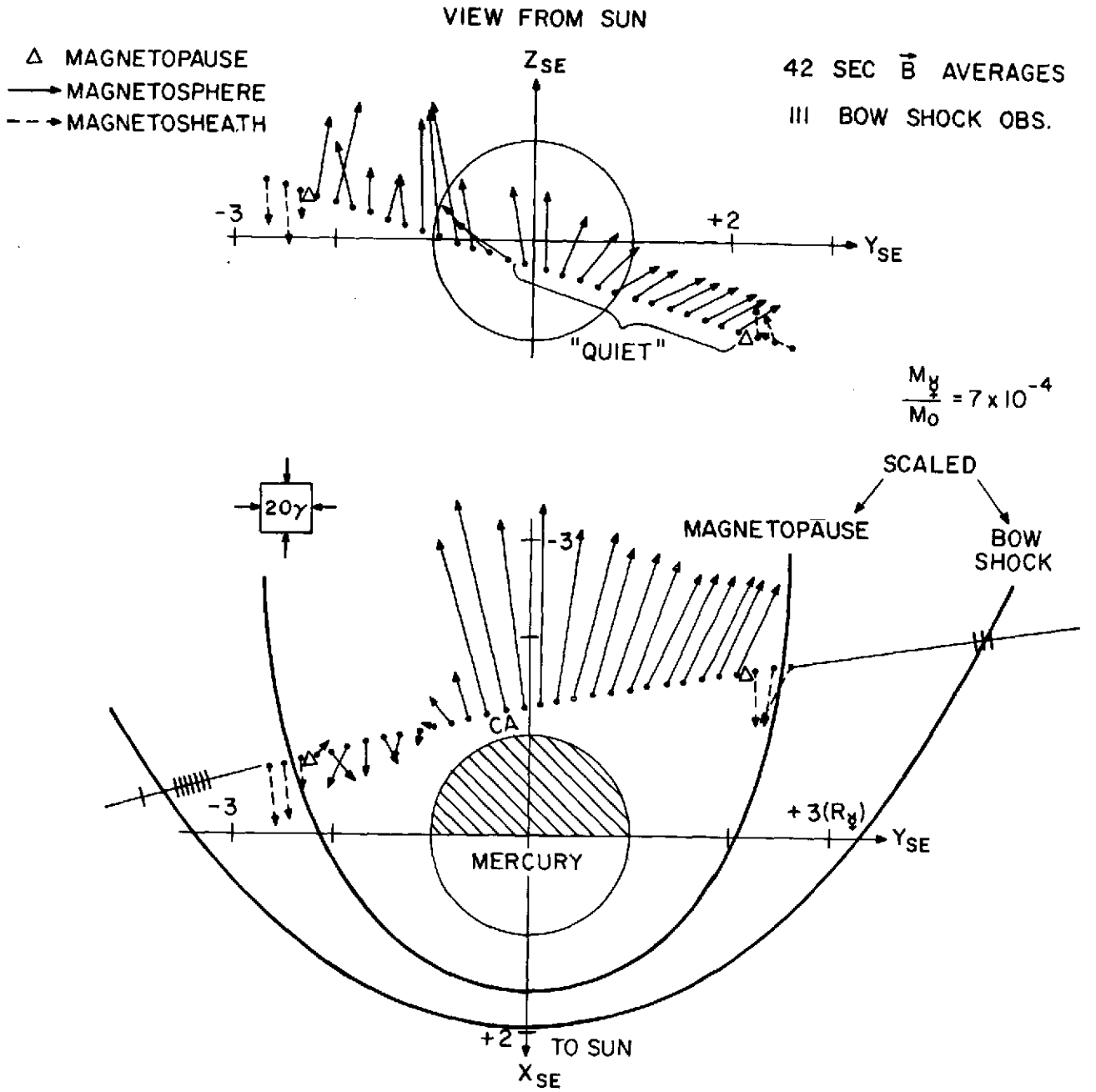


MARINER 10 MERCURY I ENCOUNTER
29 MARCH 1974

FIGURE 2

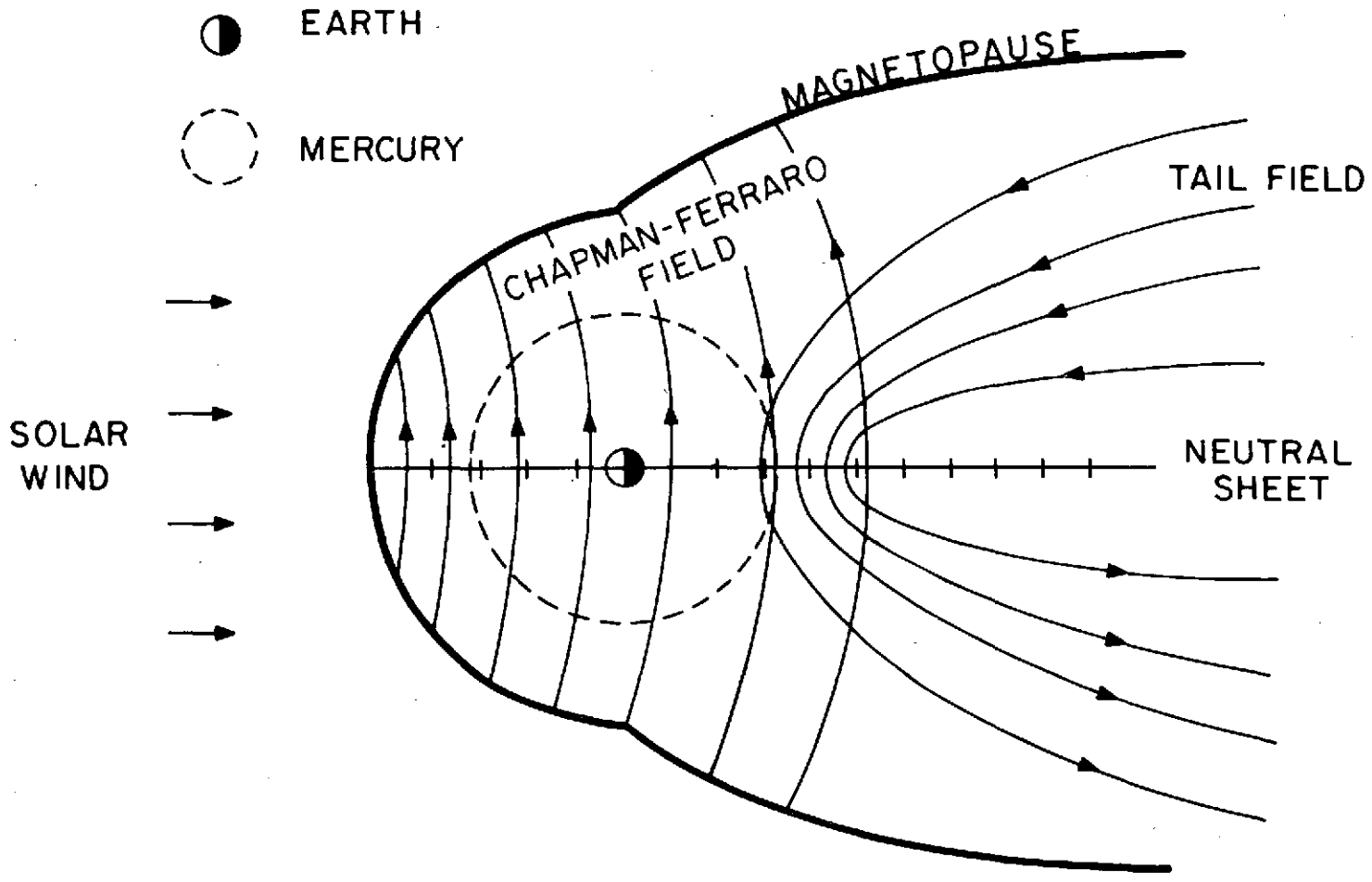
EARTH
MERCURY
MAGNETOPAUSE
TAIL FIELD
CHAPMAN-FERRARO
FIELD
SOLAR
WIND
NEUTRAL
SHEET

FIGURE 3

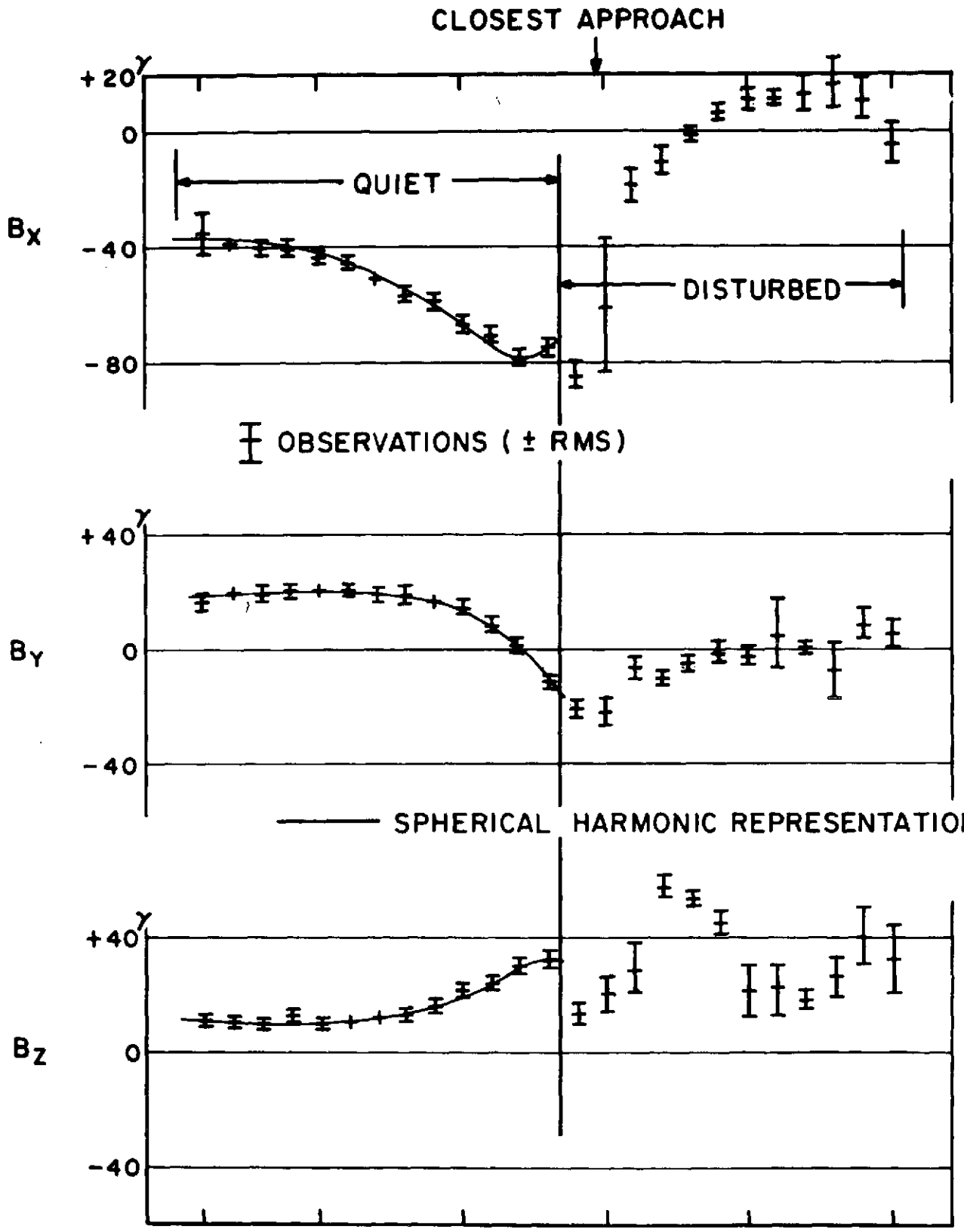


MARINER 10 MERCURY I

FIGURE 4

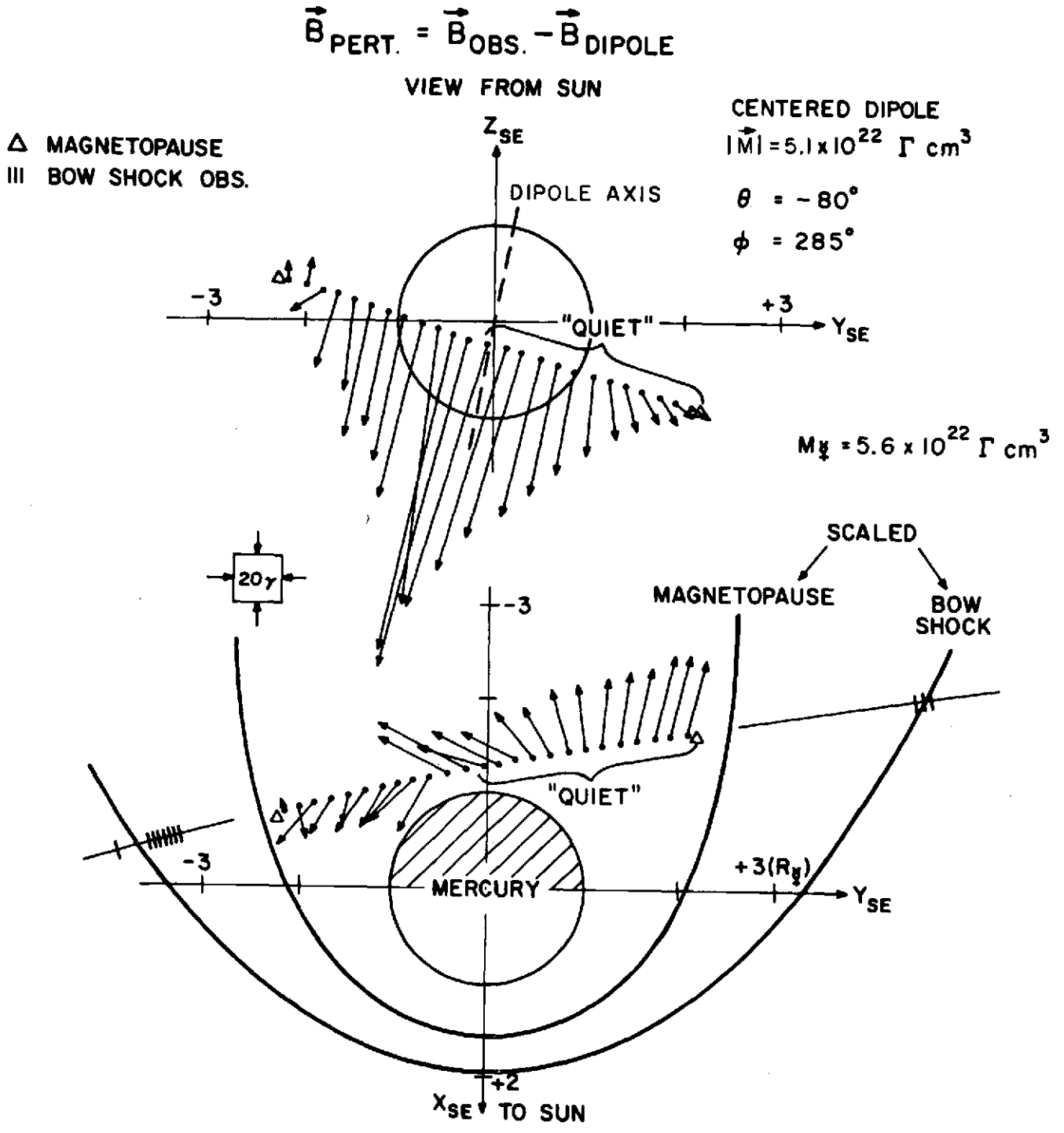


MARINER 10 MERCURY I ENCOUNTER
29 MARCH 1974

FIGURE 5

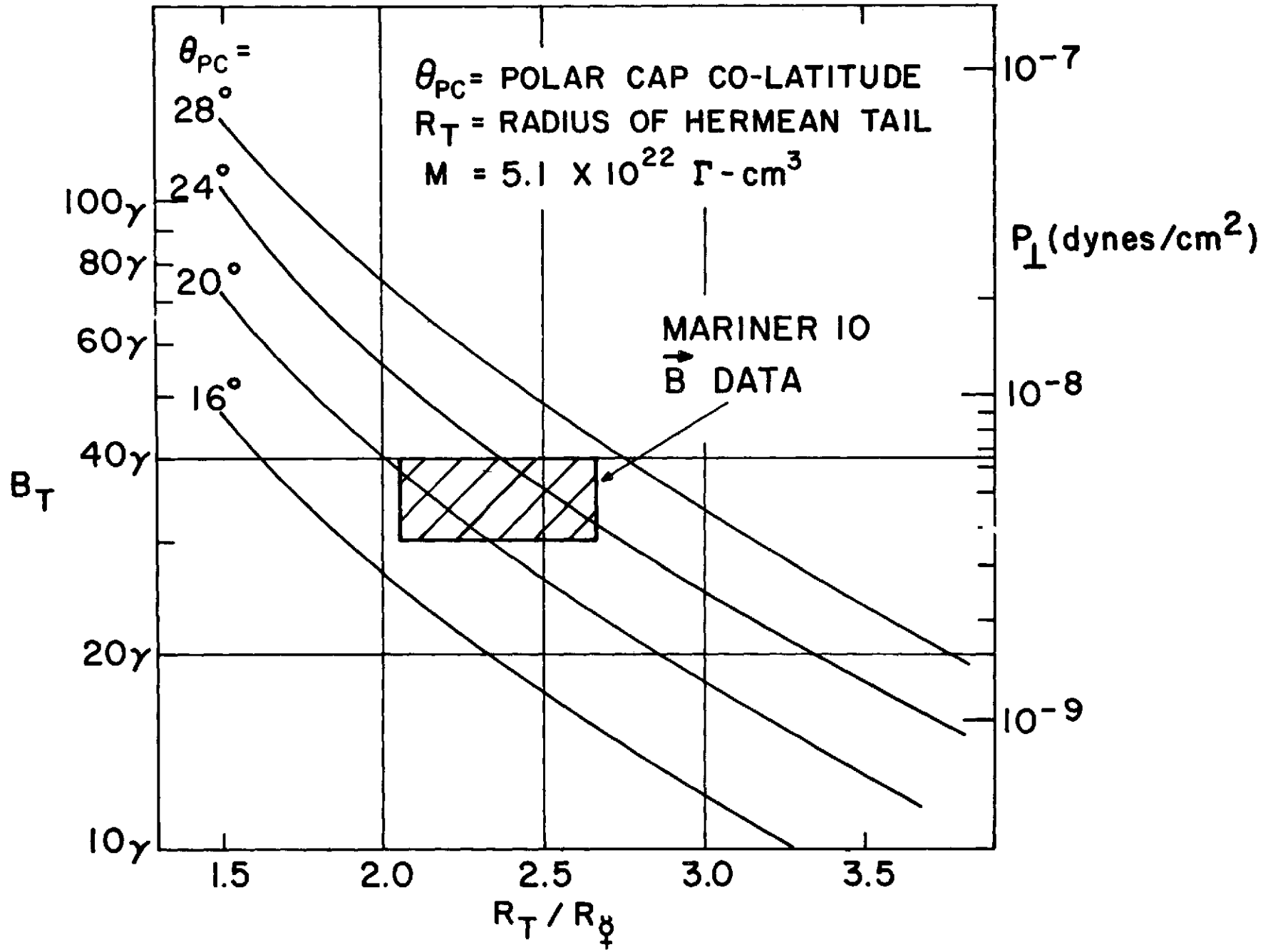
$\theta_{PC}$ =
28°
24°
20°
16°
$\theta_{PC}$ = POLAR CAP CO-LATITUDE
$R_T$ = RADIUS OF HERMEAN TAIL
M = 5.1 X $10^{22}$ Γ-cm$^3$
MARINER 10
$\vec{B}$ DATA
100γ
80γ
60γ
40γ
20γ
10γ
$B_T$
$10^{-7}$
$10^{-8}$
$10^{-9}$
$P_\perp$ (dynes/cm$^2$)
1.5
2.0
2.5
3.0
3.5
$R_T / R_\varnothing$

FIGURE 6

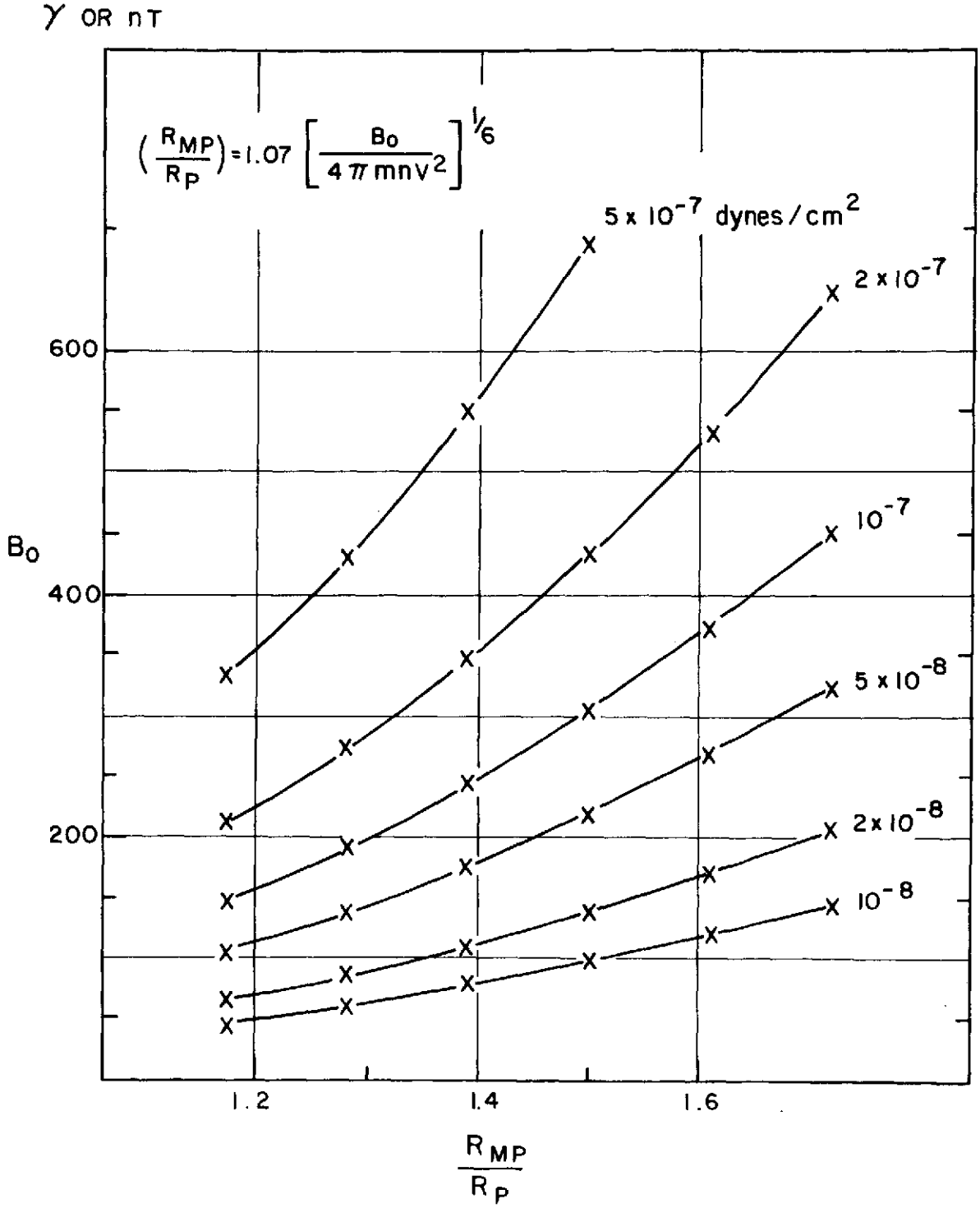
γ OR nT
$\left(\frac{R_{MP}}{R_P}\right) = 1.07 \left[\frac{B_0}{4\pi mnv^2}\right]^{1/6}$
5 x 10⁻⁷ dynes / cm²
2 x 10⁻⁷
10⁻⁷
5 x 10⁻⁸
2 x 10⁻⁸
10⁻⁸
600
400
200
B₀
1.2
1.4
1.6
$\frac{R_{MP}}{R_P}$

FIGURE 7